

Article

Performance and Capacity Optimization for High Speed Railway Communications Using UAV-IRS Assisted Massive MIMO System

Ziyue Liu ^{1,2,3}, Mingxi Yang ¹, Jingjing Cui ^{4,*}, Yue Xiao ⁵ and Xuejun Zhang ⁶

- ¹ School of Aeronautics and Astronautics and Engineering Research Center of Intelligent Air-Ground Integrated Vehicle and Traffic Control, Ministry of Education, Xihua University, Chengdu 610039, China; liuziyue_2006@126.com (Z.L.); yangmx2000@126.com (M.Y.)
- ² The Beihang University International Center for Innovation in Western China, Chengdu 610218, China
- ³ National Center of ATC Surveillance and Communication System Engineering Research, Chengdu 610199, China
- ⁴ School of Electronics and Computer Science, University of Southampton, Southampton SO17 1BJ, UK
- ⁵ Provincial Key Lab of Information Coding and Transmission, Southwest Jiaotong University, Chengdu 610031, China; alice_xiaoyue@hotmail.com
- ⁶ School of Electronic and Information Engineering, Beihang University, Beijing 100191, China; zhxj@buaa.edu.cn
- * Correspondence: jingj.cui@soton.ac.uk

Abstract: In this paper, we study the communication performance of applying unmanned aerial vehicles (UAVs) combined with intelligent reflective surfaces (IRS) in a high speed railway (HSR) scenario. This study investigates the design and performance of (multiple-input-multiple-output) MIMO systems with UAV and IRS assistance technology in high-mobility scenarios. Direct links between base stations (BS) and trains are often obstructed in suburban environments, especially in mountainous areas. We mount the IRS on the UAVs so that it can assist in the communication between the trains and the BS. With the help of the UAV-IRS, straight-line links can be established effectively, which greatly improves communication for train passengers. This paper considers the employment of large-scale antenna arrays at both the BS and train ends. Train passengers communicate with UAVs via antennas assembled on the roof of the train as gateways, which in turn communicate with the BS. We consider two types of antenna layouts on the train: all antennas are located in the center of the train named Co-located antennas (CA) layout and uniformly distributed along the train called distributed antennas (DA) layout. We can obtain the analytical up-link capacity by averaging over all locations in a cell for the above two layouts by considering the radio frequency consumption. Overall, the CA layout is found to be a better option for trains when attempting to maximize cell mean value of capacity, and DA layout achieves a more uniform distribution of capacity over the entire cell. Ultimately, the best solution will depend on the specific requirements and constraints of the selected deployment scenario.

Keywords: unmanned aerial vehicles; intelligent reflective surface; high speed railway; massive MIMO; UAV-mounted IRS; capacity optimization



Citation: Liu, Z.; Yang, M.; Cui, J.; Xiao, Y.; Zhang, X. Performance and Capacity Optimization for High Speed Railway Communications Using UAV-IRS Assisted Massive MIMO System. *Electronics* **2023**, *12*, 2547. <https://doi.org/10.3390/electronics12112547>

Academic Editor: Adão Silva

Received: 13 April 2023

Revised: 8 May 2023

Accepted: 8 May 2023

Published: 5 June 2023



Copyright: © 2023 by the authors. Licensee MDPI, Basel, Switzerland. This article is an open access article distributed under the terms and conditions of the Creative Commons Attribution (CC BY) license (<https://creativecommons.org/licenses/by/4.0/>).

1. Introduction

Due to their rapid development, high-speed railways (HSRs) are now known for their speed, comfort, safety, and reliability, as well as their ability to carry heavy loads while consuming minimal energy [1]. According to the International Union of Railways, the expansion of the global HSR network is expected to exceed 80,000 km by 2030–2035. This presents a significant challenge in meeting the demanding standards for quality service [2]. In the wireless communication system design, coverage area plays a crucial role in determining the deployment of the communication infrastructure.

We are increasingly inseparable from HSR systems in our daily lives. This has resulted in the growing demand for broadband mobile communication services on trains. The low latency and high bandwidth requirements for network services in high mobility environments and complex suburban conditions may not be met by traditional wireless communication infrastructure.

Design and performance of multiple-input-multiple-output (MIMO) systems can be enhanced by utilizing unmanned aerial vehicles (UAVs) and intelligent reflective surfaces (IRS). UAVs have the potential to improve HSRs' performance and support high-speed data transmission. Furthermore, integrating IRS with UAVs on a single platform can enhance spectrum efficiency and individual energy efficiency, extend network coverage, and provide flexible deployment options.

In recent years, the problems posed by broadband wireless communications in HSR systems have forced many new transmission technologies and architectures to be proposed [3–5]. In order to ensure high-speed data transmission for passengers, wireless communication technology plays an important role in high-speed railway systems [6]. On the one hand, the high loss of penetration caused by the rail car chassis has caused numerous problems for communication in high-speed rail systems [7]. We have come up with a solution for this problem; namely, to use antennas mounted on top of railway vehicles in a two-step hierarchical configuration. All users contact the base station (BS) using an external antenna as a relay gateway. On the other hand, communication blackouts can occur within the system in complex HSR travel scenarios, such as mountainous areas, tunnels, U-grooves, etc. [8]. In these areas where communication needs are pressing, UAVs can be rapidly deployed as air BSs to establish temporary data links with relay gateways.

An IRS consists of a set of intelligent reflective elements. Each of its original elements can independently perform the task of improving the quality of the initial received signal [9]. Because it can intelligently change the propagation channel of wireless signals, it is considered a potential communication technology [10]. Furthermore, combining IRS with UAVs and changing the signal transmission path through the IRS installed on the UAVs can create a stronger LoS path between the train and the BS, thus improving communications performance, which is the issue studied in this article.

1.1. Prior Work

Over the past few years, there has been increasing interest in developing massive MIMO UAV systems in cellular wireless networks aimed at improving the connectivity and coverage of HSR. A two-link configuration with a relay on the train makes the performance more efficient, and more antennas are expected to further improve the system performance [11]. HSR communication uses MIMO systems. HSR communication system performance can be improved by multiplexing gain or diversity gain. Massive MIMO technology is particularly well-suited for HSR communications involving UAVs, base stations, and trains of large size. The authors in [12] explored the vehicle-to-ground millimeter wave (mmWave) communication system and proposed a UAV and relay scheme, which effectively overcomes link-blocking and improves channel quality. In addition, applying UAVs to emergency communications is an innovative technology. The majority of these studies are centered on inter-UAV communication or the relay performance of UAVs. An application-based communication strategy for providing signaling services with the help of UAVs in case of emergency communication disruption in HSR is proposed to meet the communication needs in emergency communication scenarios [13].

In the event of maintenance obstructing the LoS connection between the BS and train relay, the quality of service (QoS) deteriorates noticeably. To ensure broadband access support for passengers, the use of IRS in train communication systems holds great potential that enables high-spectrum, highly reliable signals. The IRS can expand its coverage area using methods that are inexpensive, simple, and consume minimal energy. To enhance the system's robustness [14,15], dynamic phase adjustment is applied to each reflection unit on the intelligent reflecting surface (IRS), and an IRS-assisted mmWave downlink

MIMO communication system in high-speed railway (HSR) scenarios is considered. Recent research has shown that in IRS-assisted HSR systems, a limited number of antennas on a base station can be utilized to achieve the desired QoS, while the IRS can be properly deployed by creating additional virtual LoS paths to combat blocking [16]. Li et al. investigated a dual IRS for MIMO systems for HSR communication to obtain reliable channel state information and improve the performance gain of the system [8].

Furthermore, for suburban environments, mounting IRS on UAVs becomes a promising solution [17–19], and a UAV–IRS network architecture with IRS mounted on UAVs is proposed. Compared with fixed-mounted IRS, the UAV–IRS is capable of providing robust line-of-sight links to ground nodes by adjusting its altitude. The combination of IRS and UAV can facilitate the development of UAV networks [20,21]; for example, [20] designed a hovering UAV-based multi-IRS model by considering both the IRS and UAV characteristics. Li et al. proposed using a UAV–IRS relay to enable performance between the BS and suburb access points by considering the weight of the IRS; to reduce the overall weight of the IRS, it is advisable to minimize the number of reflective elements employed [21]. In [22], the authors investigated the optimization problem of UAV altitude and element quantity in conjunction with a UAV–IRS system. This paper also delves into the application of UAV–IRS technology in HSR communications, aiming to enhance capacity performance between base stations and train passengers within suburban blind spots.

The linear topology of the HSR system enables the use of a combination of MIMO and DAS (distributed antenna system) technologies. This is achieved by using optical fibers to connect remote antenna units to the central unit in a linearly distributed manner. This can also be applied on trains [23]. Furthermore, the intricate wireless propagation environment in HSR scenarios, including viaducts, tunnels, and plains, means that the UAV–IRS creates a strong LoS path and limited multi-path scatter, which is known as Rician fading [24]. MIMO and DAS technologies can help overcome the challenges of Rician fading by using multiple antennas to improve signal quality and distributing antennas to cover a wider area. These technologies can improve the performance of HSR communication systems, increasing data rates and reliability of wireless links, especially in challenging environments, and will become increasingly important as demand for high-speed and reliable communication in HSR continues to grow.

1.2. Motivation and Contributions

As mentioned above, in this paper, we propose an IRS-assisted UAV–HSR network, where the IRS is mounted on the UAV and utilized to extend the communication range in case of HSR signal blockage, without building a new infrastructure. We consider the optimal design solution for the IRS-assisted UAV–HSR communication system with massive MIMO as well as a system with massive antennas at both the transceiver and the transmitter.

The objective of this paper is to design an optimal high-speed railway communication system and evaluate the capacity of the UAV–train communication link, based on the aforementioned issues. To achieve this, we consider a dual-link high-speed railway communication system in which both BS and train relays have a large number of antennas to achieve high data rates in high-speed railway systems. Our contributions are four-fold.

- (1) This is the first study of how to use UAV–IRS systems to enhance scenes along high-speed railways. The system establishes LoS links through UAV–IRS to bypass environmental obstacles such as hills and trees to fill in the communication blind spots.
- (2) The UAV–IRS HSR system, with either a DA or a CA layout, is calculated by taking into account various factors such as radio frequency power loss, small-scale fading, large-scale fading, and antenna geometry. This calculation involves averaging the up-link capacity over all locations within the whole cell.
- (3) Our analysis shows that the mean value of the up-link capacity for the co-located layout exhibits a concave relationship with respect to the number of transmitting antennas. Hence, we can obtain an optimal quantity of antennas. It maximizes the mean value of the up-link capacity. This is obtained by finding the extreme value

of this function. For the distributed antenna on the train, upper- and lower-bound functions were established for the mean value of up-link capacity, which enables the determination of the optimal or sub-optimal number of antennas.

- (4) According to numerical and simulation results, the capacity of cells in a cellular network is higher on average in a CA layout. However, in a DA layout, the capacity is more evenly distributed across different cell locations.

1.3. Organization

The subsequent sections of this document are structured as follows. Section 2 presents the system architecture based on UAV-IRS in detail; Section 3 gives the up-link ergodic capacity of massive MIMO systems with a channel based on UAV-IRS; the optimum designs for systems with DA or CA layouts are identified in Section 4; and Section 5 gives the theoretical and simulation results, while Section 6 provides concluding remarks for this paper. The notation used in this article is given in Table 1.

Table 1. Notation.

Notation	Description
I_n	The identity matrix of dimension is n
$E_{r,t}$	The all-ones matrix with dimensions $r \times t$
$H(\cdot)$	The conjugate transpose operation
CN	The complex Gaussian and Gaussian distributions
σ^2	The variance of the Gaussian
$\mathbb{E}(\cdot)$	The expectation operator
h_r	The value assumed for the height of the train relay
h_u	The position referred to is in the center of the cell
L_t	The total length of the train
d_m	The distance from the base station to the m -th antenna
u_m	The m -th MG antenna's position on the train
G	The channel 1 BS \rightarrow UAV-IRS from BS to UAV-IRS
H	The channel 2 UAV-IRS \rightarrow MG from UAV-IRS to MG
n	The added additive white Gaussian noise (AWGN)
f_c	The carrier frequency
d	The distance between UAV-MG
$\Lambda(x)$	As a diagonal matrix, where the n -th element represents $\rho_n(x)$
α	The time correlation factor
W_n	Complex Gaussian noise matrix
P	The total transmission power at the disposal of the transmitter
β	Simulation of hardware power consumption of transmitting antennas
UAV	Unmanned aerial vehicle
IRS	Intelligent reflective surfaces
BS	Base station
CA	Co-located antennas
DA	Distributed antennas
HSR	High-speed railways
MIMO	Multiple-input-multiple-output

The notation used in this paper follows a specific convention, where lowercase boldface notation denotes vectors and uppercase boldface denotes matrices. The identity matrix of dimension is n represented as I_n ; the all-ones matrix with dimensions $r \times t$ is denoted by $E_{r,t}$; and the conjugate transpose operation is indicated by $H(\cdot)$. The complex Gaussian and Gaussian distributions are denoted as CN. The mean variance is σ^2 . The expectation operator is $\mathbb{E}(\cdot)$.

2. System Model

Consider an unmanned aircraft-assisted railway communication system. This system uses a two-tier network architecture as shown in Figure 1.

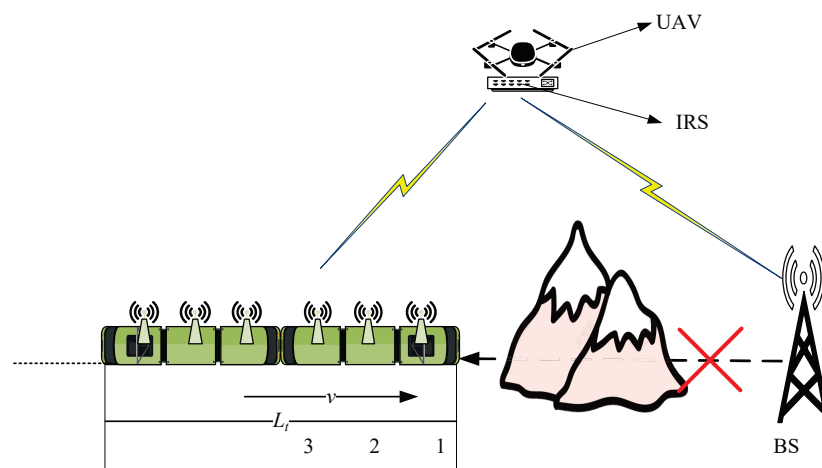


Figure 1. The use of IRSs has assisted in implementing massive MIMO technology in the complex and high-speed environment of railway scenarios.

We set the UAV as a base station (BS). The position referred to is in the center of the cell with height h_u , which is intended to provide the ability to serve all users on the train. The train is furnished with a mobile gateway (MG), and this mobile gateway is furnished with some antennas [11,25] for communication. The value we assume for the height of the train relay is h_r meters. The value L_t represents the total length of the train under consideration. The train starts moving from the cell along the velocity direction. User equipment (UE) on the train that wants to connect to the BS has to use the mobile gateway, and the MG provides network coverage for the train passengers. Additionally, both the MG and the UE are not moving much relative to one another. Therefore, the optimal design of the UAV–MG link that limits the performance of the entire system is the focus of our attention. The train may operate on a distinct frequency band from that of the UAV–MG link, as long as the MG–UE link only provides coverage. To avoid interference between two levels of communication, we improve the capability of the UAV–MG. We use $N \gg M$ UAV–IRS in the system.

In this paper, considering the complex train operating environment, we make the assumption that there exist obstacles along the direct path from BS to MG, thereby obstructing said path. In order to guarantee that the signal between the BS and the MG has a pathway, we look at the typical HSR communication system with the help of the IRS shown in Figure 2. The UAV–IRS consists of some reflective elements mounted on the UAV. The equivalent channel of the communication links, $BS \rightarrow UAV\text{-IRS} \rightarrow MG$, channel 1 $BS \rightarrow UAV\text{-IRS}$ from BS to UAV–IRS, and then the other channel 2 $UAV\text{-IRS} \rightarrow MG$ from UAV–IRS to MG, are expressed as \mathbf{H} , \mathbf{G} . Assuming that the communication of channel 1 has the perfect link, we focus on the capacity of the data transmitted by channel 2. Furthermore, it is assumed that the UAV–IRS can reflect the channel perfectly, which makes it look like an LoS channel between the MG and the base station.

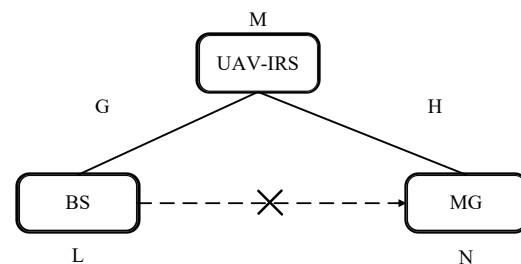


Figure 2. System model with UAV–IRS high-speed railway.

Assuming the base station’s (BS) horizontal coordinate is 0, the train’s tail-end horizontal coordinate is x . When the train enters the cell, the tail coordinates of the train are 0.

We can then obtain the equation $x = vt$, where v represents the speed of the train. Using this equation, the distance from the base station to the m -th antenna can be calculated as:

$$d_m(x) = \sqrt{(h_u - h_r)^2 + u_m^2(x)}. \tag{1}$$

In the previous equation, the m -th MG antenna's position on the train can be described by its horizontal coordinate $u_m(x)$ and, if the MG antennas are evenly spaced out along the length of the train, then $u_m(x) = x + \frac{(m-1)L}{M-1}$, for $m = 1, \dots, M$.

The up-link signal from the mobile device to the base station (MG-BS system) is considered. The result of this processing is that the equivalent discrete-time signal received by the base station is:

$$\mathbf{y} = \mathbf{G}\mathbf{x} + \mathbf{n}. \tag{2}$$

The equation describes a communication system with a MIMO channel, where the output vector $\mathbf{y} = [y_1, \dots, y_N]^T \in \mathcal{C}^{N \times 1}$. The input vector is $\mathbf{x} = [x_1, \dots, x_M]^T \in \mathcal{S}^{M \times 1}$. The added additive white Gaussian noise (AWGN) is $\mathbf{n} = [n_1, \dots, n_N]^T$. In this equation, the vector has a mean of zero and a covariance matrix $\sigma_0^2 \mathbf{I}_N$, and $\mathbf{G} \in \mathcal{C}^{N \times M}$ is the channel coefficient matrix. It is set through the distance vector $\mathbf{d}(x) = [d_1(x), \dots, d_M(x)]^T$. The input vector satisfies the power constraint for input $\mathbb{E}(\mathbf{s}^H \mathbf{s}) + M\beta \leq P_0$. In the previous equation, P_0, β represent the total transmit power available to the transmitter and the additional power loss used to simulate the transmit antenna, respectively. There are many factors that constitute additional power loss. The most prevalent issue in radio frequency (RF) circuits is power loss resulting from power consumption and amplifier inefficiency [26].

\mathbf{G} is a channel coefficient matrix that takes into account the fading effects of small and large scales. (m, n) -th is an element of \mathbf{G} and can be expressed as

$$g_{mn}(x) = \sqrt{\rho_m(x)} \times h_{mn}. \tag{3}$$

The signal strength of the m -th relay station on a train, called the large-scale fading factor ρ_m , depends on its location. The small-scale attenuation coefficient h_{mn} , which represents the signal loss between the n -th transmitting antenna and the m -th, is assumed to be independent and identically distributed (i.i.d).

We propose several models for the current air-to-ground channels. The radio signal suffers from free space propagation losses. Not only that, it also suffers losses due to shadows and scattering from the urban environment. Here we deal with some problems, including mean path loss and the random shading problem. The equation comprises two components: one denotes the path loss of an LoS link, while the other signifies the path loss of an NLoS link [27]:

$$PL_{LoS} = \left(\frac{c}{4\pi f_c d(x)} \right)^2 \eta_L, \tag{4}$$

$$PL_{NLoS} = \left(\frac{c}{4\pi f_c d(x)} \right)^2 \eta_{NL}. \tag{5}$$

We can derive from (1) that the carrier frequency and velocity of light are indicated by f_c and c , and $d(x)$ is the distance between UAV-MG. In addition to this, the mean additional losses for LoS and NLoS are η_L and η_{NL} , (10, 0.5), as given in [28].

We must have knowledge of the terrain to determine whether it is an LoS link or an NLoS link. In summary, we look at the probability of the average path loss. The average value is established from the LoS and NLoS conditions and is expressed as:

$$C_{PL} = PL_{LoS} Pr_{LoS} + PL_{NLoS} Pr_{NLoS}, \tag{6}$$

where Pr_{LoS} and Pr_{NLoS} represent the probabilities of establishing LoS and NLoS connections between the MG and UAV-IRS. The probability of LoS can be given by [28]:

$$Pr_{LoS} = \frac{1}{1 + \alpha_1 \exp[-\alpha_2(\eta - \alpha_1)]}, \tag{7}$$

where parameter α_1 and α_2 are given in [28] and $\eta = \arctan(h_u/d_m)$ is the angle between UAV-IRS and MG. The shading is assumed to follow the log-normal distribution, i.e., $\log(S_n) \sim \mathcal{N}(0, \sigma_n^2)$.

We decompose the channel coefficient matrix, i.e., \mathbf{G} , as:

$$\mathbf{G} = \mathbf{H}\Lambda(x)^{1/2}. \tag{8}$$

The given paragraph describes a small-scale fading matrix denoted by $\mathbf{H} \in \mathcal{C}^{N \times M}$, where h_{mn} is an element in (m, n) -th. $\Lambda(x) = \text{diag}\{\rho_1(x), \dots, \rho_M(x)\} \in \mathcal{C}^{M \times M}$ is also referred to as a diagonal matrix, where the n -th element represents $\rho_n(x) = S_n C_{PL}$.

Let $\gamma = \mathbf{E}[h_{n-1}, h_n]$ denote the time correlation factor [29]. It is determined by the Bessel function, shown as:

$$\gamma = J_0(2\pi f_c \tau v / c), \tag{9}$$

where $J_0(\cdot)$ denotes a function that is a zero-third order Bessel function of the first class. The carrier frequency is f_c . The length of time between two sampled instances is τ ; v is the speed of the train; and c denotes the speed of light.

In a UAV-aided HSR system, the spectral efficiency performance of the conversion receiver is degraded. The reason is that it is in a highly mobile environment. A particularly important part of the communication bandwidth is the Doppler shift, especially in UAV-aided HSR systems. Thus, the channel can be modeled with the effective time correlation, and the fading coefficient matrix \mathbf{H} can be expressed as:

$$\mathbf{H}_n = \alpha \mathbf{H}_{n-1} + \sqrt{1 - \alpha^2} \mathbf{W}_n, \tag{10}$$

where \mathbf{H}_{n-1} is the $(n - 1)$ th channel matrix, and \mathbf{W}_n is a complex Gaussian noise matrix that is independent at \mathbf{H}_{n-1} .

The input vector satisfies $\mathbb{E}(\mathbf{s}^H \mathbf{s}) + M\beta \leq P$. The total transmission power at the disposal of the transmitter is P . β is then used to model the hardware power consumption of a transmitting antenna. There are many factors that can affect the value of β ; for example, the power consumption of the RF circuit and the power dissipation caused by amplifier inefficiency.

The ergodic capacity of the MIMO system in the up-link channel is referred to [30]:

$$\begin{aligned} C(x) &= \mathbb{E} \left[\log_2 \det \left(\mathbf{I}_N + \frac{P_0 - \beta M}{M\sigma_0^2} \mathbf{G}\mathbf{G}^H \right) \right] \\ &= \mathbb{E} \left[\log_2 \det \left(\mathbf{I}_M + \frac{P_0 - \beta M}{M\sigma_0^2} \Lambda(x)^{1/2} \mathbf{H}^H \mathbf{H} \Lambda(x)^{1/2} \right) \right], \end{aligned} \tag{11}$$

where the expectation is not only fading on a small scale but also shading on a large scale. The variance of AWGN is σ_0^2 . A second equation can be derived from the determinant identity $\det(\mathbf{I} + \mathbf{A}_1 \mathbf{A}_2) = \det(\mathbf{I} + \mathbf{A}_2 \mathbf{A}_1)$.

3. Statistical Modeling of Up-Link Capacity in a Fading Channel

In the following, by analyzing the CA and DA designs on a train, we determine optimal M values to increase the mean value of cell capacity.

To make things easier to understand and evaluate, as a first step we have to precisely estimate the mean up-link capacity. In a massive multiple-input-multiple-output system

$N \gg M$, the small scale fading can be modeled with Rician fading. The coefficient matrix can be expressed as

$$\mathbf{H} = a_1 \mathbf{H}_{\text{LoS}} + a_n \mathbf{H}_{\text{NLoS}}, \tag{12}$$

where $a_1 = Pr_{\text{LoS}}$ and $a_n = 1 - a_1$. The matrix \mathbf{H}_{LoS} and \mathbf{H}_{NLoS} are contributed by LoS and NLoS components, respectively. Thus, they are all-one matrix and i.i.d Gaussian distributed with zero mean and unit variance.

Based on the analysis in Ref. [31], when N is large, the product matrix can be approximated by

$$\mathbf{H}^H \mathbf{H} \approx Na_1 \mathbf{E}_{M,M} + Na_n \mathbf{I}_M, \tag{13}$$

and the determinant of $\mathbf{H}^H \mathbf{H}$ can be given by

$$\det(\mathbf{H}^H \mathbf{H}) = N(Ma_1^2 + a_n^2) (a_n^2)^M. \tag{14}$$

With the above results, the up-link capacity in (11) can be represented as

$$C(x) \approx \mathbb{E}_{S_n} \left[\log_2 \det \left(\mathbf{I}_M + \frac{P_0 - \beta M}{M\sigma_0^2} N(Ma_1^2 + a_n^2) (a_n^2)^M \Lambda(x) \right) \right], \tag{15}$$

the lognormal random variable (RV) is S_n , where the expectation is performed. We know that $\mathbb{E}[\mathbf{H}_{\text{NLoS}}^H \mathbf{H}_{\text{NLoS}}] = N\mathbf{I}_M$, $\mathbb{E}[\mathbf{H}_{\text{LoS}}^H \mathbf{H}_{\text{NLoS}} + \mathbf{H}_{\text{NLoS}}^H \mathbf{H}_{\text{LoS}}] = \mathbf{0}$ and Jensen's inequality is $\mathbb{E}[\log_2 \det f(\mathbf{H})] \leq \log_2 \det \mathbb{E}[f(\mathbf{H})]$, so the upper bound of $C(x)$ is the right-hand part of (15).

In the condition of high signal-to-noise ratio, we can further simplify (15) to:

$$C(x) \approx M \log_2 \left(\frac{P_0 - \beta M}{\sigma_0 M} \right) + (M - 1) \log_2 (a_n^2 N) + \log_2 (a_1^2 NM + a_n^2 N) - \alpha \sum_{n=1}^M \log_2 (d_n(x)). \tag{16}$$

We know that S_n satisfies $\log(S_n) \sim \mathcal{N}(0, \sigma_n^2)$, which means that S_n satisfies a log-normal distribution. The reason that large-scale shading has no effect on the traversal ability is that we have $\mathbb{E}_{S_n}[\log_2(S_n)] = 0$.

Subsequently, we can calculate the mean value of capacity within the cell, which is expressed as

$$\bar{C} = \frac{v}{2D} \int_{-L/2/v}^{(2D-L/2)/2} C(x) dx. \tag{17}$$

The number of M antennas is inversely proportional to the $C(x)$ and \bar{C} capacity. By increasing the system's multiplexing gain, we can enhance its capacity as the number of M increases. If we blindly increase the number of M , it will cause greater circuit power consumption and overhead, thus losing power. Therefore, it is important to choose the correct M value for the HSR communication system.

4. Optimization Problems

In this section, by considering the co-located antenna and distributed antenna layout, the optimal value of M is determined. We can write the optimization problem as:

$$\begin{aligned} &\text{maximize} && \text{The mean value of cell capacity with respect to the antenna number } M \\ &\text{s.t.} && P_0 \leq P_t. \end{aligned}$$

We will consider two layouts to solve this optimization problem, as shown below.

4.1. Co-Located Antenna Layout

If all of the antennas are mounted at the train’s rear or center, in a co-located configuration, we have $d_1(x) = \dots = d_M(x) = \sqrt{z^2 + (x + L/2)^2}$. In this situation, we can simplify the mean value of cell capacity obtained from (16) as:

$$\begin{aligned} \bar{C}_{CA} = & M \log_2 \left(\frac{P_0 - \beta M}{\sigma_0^2 M} \right) + (M - 1) \log_2 (a_n^2 N) \\ & + \log_2 (a_1^2 NM + a_n^2 N) - \frac{\alpha M}{4D} \int_{-D}^D \log_2 (z^2 + x^2) dx. \end{aligned} \tag{18}$$

Define $h(a) = \int_{-D+a}^{D+a} \log_2 (z^2 + x^2) dx$. By using integration by part, we can solve this integral and obtain:

$$h(a) = \frac{1}{\log 2} [g(a) + g(-a) - 4D], \tag{19}$$

where

$$g(a) = (D + a) \log [(D + a)^2 + z^2] + 2z \arctan \left(\frac{D + a}{z} \right). \tag{20}$$

We combine (18) and (19) together to get:

$$\bar{C}_{CA} = M \log_2 (A_1 / M - A_2) + F_1 M + \log_2 (a_1^2 MN + a_n^2 N) - \log_2 (a_n^2 N), \tag{21}$$

where $A_1 = \frac{P_0}{\sigma_0^2}$, $A_2 = \frac{\beta}{\sigma_0^2}$, and $F_1 = \log_2 (a_n^2 N) - \frac{\alpha}{4D} h(0)$.

The conclusion drawn from Equation (21) is that, for co-located antennas, the value of M must satisfy either the condition $\frac{A_1}{M} - A_2 > 0$ or $P_0 > \beta M$, indicating that the total power loss of the transmitting antenna system does not exceed the available power. From this, we can obtain the range of M , i.e., $0 < M < \frac{P_0}{\beta} = \frac{A_1}{A_2}$.

We relax the range of values of M to a positive real number so that we can identify the optimal value of M that maximizes \bar{C}_{CA} through analysis. The optimal value of M that maximizes \bar{C}_{CA} can be obtained by calculating the first-order derivative of \bar{C}_{CA} with respect to M , if we allow the range of values for M to be any positive real number. The first derivative of \bar{C}_{CA} with respect to M can then be expressed as:

$$\frac{\partial \bar{C}_{CA}}{\partial M} = \log_2 \left(\frac{A_1}{M} - A_2 \right) - \frac{1}{\log 2} \frac{A_1}{A_1 - A_2 M} + F_1 + \frac{1}{\log 2} \frac{a_1^2 N}{a_1^2 NM + a_n^2 N}. \tag{22}$$

By the previous equation, we can conclude that the second-order derivative of \bar{C}_{CA} with respect to M is:

$$\frac{\partial^2 \bar{C}_{CA}}{\partial M^2} = -\frac{1}{\log 2} \cdot \left[\frac{A_1^2}{(A_1 - A_2 M)^2 M} + \frac{a_1^4 N^2}{(a_1^2 NM + a_n^2 N)^2} \right], \tag{23}$$

With $\frac{\partial^2 \bar{C}}{\partial M^2} < 0$ from (23), we have that \bar{C}_{CA} is concave if the domain of definition is M .

By determining the concavity of the \bar{C}_{CA} as regards M , we can find the maximum value of \bar{C}_{CA} and obtain the value of M that maximizes the C:

$$\left. \frac{\partial \bar{C}}{\partial M} \right|_{M=\tilde{M}} = 0, \tag{24}$$

with (22), and denoting \tilde{M} as the solution. We can obtain \tilde{M} by relaxing M as a real number.

Because \bar{C}_{CA} is concave in M , \bar{C}_{CA} has a non-negative slope at $M = (\lfloor \tilde{M} \rfloor)$. When $\epsilon \geq 0$, $\bar{C}_{CA} (\lfloor \tilde{M} \rfloor) \geq \bar{C}_{CA} (\lfloor \tilde{M} \rfloor - \epsilon)$. We can similarly deduce that $\bar{C}_{CA} (\lceil \tilde{M} \rceil) \geq \bar{C}_{CA} (\lceil \tilde{M} \rceil + \epsilon)$

because of the positive slope of \bar{C}_{CA} at $M = \lceil \tilde{M} \rceil$. From the above analysis, we know that $\lfloor \tilde{M} \rfloor$ or $\lceil \tilde{M} \rceil$ will be the best integer value of M . Therefore, we can obtain the optimal value of M , denoted as:

$$\hat{M} = \arg \max M \in \{ \lfloor \tilde{M} \rfloor, \lceil \tilde{M} \rceil \} \bar{C}_{CA}(M). \tag{25}$$

Although the approximate solution \tilde{M} is obtained through a relaxation technique using real numbers, we can still calculate the exact integer optimal value \hat{M} by applying Equation (25).

4.2. Distributed Antenna Layout

Assuming a uniform distribution of antennas along the train, the distance between the BS and the k -th MG antenna can be expressed as follows: $d_k(x) = \sqrt{z^2 + (x + v_k)^2}$, where $v_k = \frac{(k-1)L}{M-1}$. From (16), calculating the mean value of cell capacity requires the integral solution. The distance between the base station and the k -th mobile gateway antenna is $d_k(x) = \sqrt{z^2 + (x + v_k)^2}$, which assumes that the antennas are evenly distributed on the train. The equation has $v_k = \frac{(k-1)L}{M-1}$. From (16), if we want to derive the mean value of capacity of the cell, we have to solve the integral:

$$S_k = \int_{-D-L/2}^{D-L/2} \log_2 [z^2 + (x + v_k)^2] dx, \tag{26}$$

in which letting $x' = x + v_k$, (19) will solve the integration problem in (26). We obtain $S_k = h(v_k - \frac{L}{2})$, which is the result after integration.

Subsequently, we can write the mean cell capacity of the distributed antenna in (16):

$$\begin{aligned} \bar{C}_{DA} = & M \log_2 \left(\frac{A_1}{M} - A_2 \right) + (M - 1) \log_2 (a_n^2 N) \\ & + \log_2 (a_1^2 MN + a_n^2 N) - \frac{\alpha}{4D} \sum_{k=1}^M h(v_k - \frac{L}{2}). \end{aligned} \tag{27}$$

From (21) and (27), there are capacity differences between the CA and DA layouts, and their differences are $Mh(0)$ and $\sum_{k=1}^M h(v_k - \frac{L}{2})$. There is a difference in the direct capacity of CA and DA layouts. From (21) and (27), the difference lies in $Mh(0)$ and $\sum_{k=1}^M h(v_k - \frac{L}{2})$.

We write the following theorem on the function $h(a)$ for comparing the performance of the systems with CA and DA layouts.

Lemma 1. $h(a)$ is a function defined in (20), and when $a \in (-D, D)$, $h(a)$ is a convex function that is even.

Proof. That $h(a)$ is an even function is easy to see from (19), and the first-order derivative of $h(a)$ is:

$$h'(a) = \log [(D + a)^2 + z^2] - \log [(D - a)^2 + z^2], \tag{28}$$

and the second derivative of $h(a)$ is:

$$h''(a) = \frac{2(D + a)}{(D + a)^2 + z^2} + \frac{2(D - a)}{(D - a)^2 + z^2}. \tag{29}$$

We can conclude that $h''(a) \geq 0$ when $a \in (-D, D)$. □

Now we introduce the differences between \bar{C}_{CA} and \bar{C}_{DA} in various aspects.

Proposition 1. We defined the layouts of CA and DA in (21) and (27), respectively, and it was concluded that the mean value of cell capacity of the CA layout surpasses that of the DA layout, i.e., $\bar{C}_{CA} \geq \bar{C}_{DA}$.

Proof. From Lemma 1, we know that since the function $h(a)$ is convex in the range of $|a| < D$ and $\frac{1}{M} \sum_{k=1}^M (v_k - \frac{L}{2}) = 0$, we can prove that $h(a)$ satisfies the criterion of convexity. Since $h(a)$ is convex, we can obtain:

$$h(0) \leq \frac{1}{M} \sum_{k=1}^M h(v_k - \frac{L}{2}). \tag{30}$$

Combining (21), (27), and (30) completes the proof. \square

Equation (27) gives the mean value of cell capacity \bar{C}_{DA} , which is not a convex function. We determine the lower bound on \bar{C}_{DA} that can help solve the optimization problem, as described below.

Corollary 1. Equation (27) provides a lower bound for the mean value of cell capacity of the DA layout, $\bar{C}_{DAL} \leq \bar{C}_{DA}$, where:

$$\begin{aligned} \bar{C}_{DA} = & M \log_2 \left(\frac{A_1}{M} - A_2 \right) + (M - 1) \log_2 \left(a_n^2 N \right) \\ & + \log_2 \left(a_l^2 MN + a_n^2 N \right) - \frac{\alpha}{4D} h \left(\frac{L}{2} \right). \end{aligned} \tag{31}$$

Proof. Since $h(a)$ is even and $h(a)$ is convex, we can infer that the upper limit of the value $h(a)$ for $a \in [-\frac{L}{2}, \frac{L}{2}]$ is $h(\frac{L}{2}) = h(-\frac{L}{2})$, and then we can deduce that $h(v_k - \frac{L}{2}) \leq h(\frac{L}{2})$ for $k = 0, \dots, M - 1$. Equation (31) is obtained by combining the above result with (27). \square

Similar to (23), in the case where M is a real relaxation, it can be demonstrated that \bar{C}_{DAL} is a concave function of M , with a first-order derivative with respect to M that is:

$$\frac{\partial \bar{C}_{DAL}}{\partial M} = \log_2 \left(\frac{A_1}{M} - A_2 \right) - \frac{1}{\log 2} \frac{A_1}{A_1 - A_2 M} + F_2 + \frac{1}{\log 2} \frac{a_l^2 N}{a_l^2 NM + a_n^2 N}, \tag{32}$$

where $F_2 = \log_2(a_n^2 N) - \frac{\alpha}{4D} h(\frac{L}{2})$.

Proposition 1 specifies the upper bound of C_{DAL} , and Corollary 1 specifies the lower bound of \bar{C}_{DAL} . When $L \rightarrow 0$, the upper and lower bounds will merge with each other. We compare the difference between the upper and lower bounds and derive:

$$\Delta \bar{C} = \bar{C}_{CA} - \bar{C}_{DAL} = \frac{\alpha}{4D} M \left[h \left(\frac{L}{2} \right) - h(0) \right]. \tag{33}$$

In the actual situation of the system, when $R \gg L$, the value of $\Delta \bar{C}$ is small. Therefore, in the practical case, the configuration of the system is tightly defined by these two bounds.

Algorithm 1 proposes a sub-optimal method for finding the value of M that maximizes \bar{C}_{DA} in Equation (27), using two bounds.

Algorithm 1 Bounds search algorithm.

- 1: Input: $P_0, \beta, \sigma_0^2, N, \alpha, L$, and D .
 - 2: STEP 1: Solve for \tilde{M} by setting $\left. \frac{\partial \bar{C}_{CA}}{\partial M} \right|_{M=\tilde{M}} = 0$ with the assistance of calculation.
 - 3: STEP 2: Solve for \check{M} by setting $\left. \frac{\partial \bar{C}_{DAL}}{\partial M} \right|_{M=\check{M}} = 0$ with the assistance of calculation and the help of (32).
 - 4: STEP 3: Find $\hat{M} = \arg \max M \in \mathcal{U} \bar{C}_{DA}$, where $\mathcal{U} = \{ \lfloor \min\{\tilde{M}, \check{M}\} \rfloor, \dots, \lceil \max\{\tilde{M}, \check{M}\} \rceil \}$.
 - 5: Output \hat{M} .
-

The bounds search algorithm conducts a search within a finite range of M , and the upper and lower limits of \bar{C}_{DA} can be derived from this range. Due to the typically small size of this range, the candidates of the search are also limited, resulting in low complexity.

5. Numerical and Simulation Results

In this section, we present numerical results that led to the development of antenna selection algorithms for both the co-located layout and the distributed layout. Furthermore, we have validated these findings through analytical verification. Table 2 shows the parameters to be used. In an outdoor scenario, 2GHz carrier frequency can expanded coverage in this scene.

Table 2. Parameters set.

AWGN power spectral density N_0	−144 dbm/Hz
The cell radius D	1000 m
The UAV altitude h_u	100 m, 200 m, 300 m
The train length L	200 m, 400 m
The bandwidth B	20 MHz
The total transmit power P_0	20 W
The RF power loss β	0.4 W, 0.5 W, 0.6 W
The BS antennas' number N	100
The carrier frequency f_c	2 GHz

Figure 3 demonstrates the correlation between the mean value of cell capacity and number of transmitting antennas for systems employing CA and DA layouts with $h_u = 200$ m. We did not use any of the following approximations in our simulations: the high SNR approximation (16) or the asymptotic orthogonal approximation (13). The UAV at higher attitude means a stronger direct path, but the lower the diversity gain. Thus the capacity is lower with the bigger h_u . However, with these two approximations, we obtained analytical results from (21), (27), and (31). For each system configuration, the simulation outcomes and the analytical results agree very well, particularly when M is small. As the value of M increases, the signal-to-noise ratio of each antenna decreases. This statement implies that the theoretical results reflect the lower bound of simulation results due to the high SNR approximation. It is very important that we conclude from the data outcomes that the mean value of cell capacity of all systems is concave. As conjectured in Proposition 1, the value of \bar{C}_{DA} is slightly lower than that of \bar{C}_{CA} , and the lower bound of \bar{C}_{DA} is used as a comparison with that of \bar{C}_{DAL} , which is quite tight. The most desirable value for both DA and CA systems is 30, which is obtained via Algorithm 1; however, the best value for the DA system via exhaustive search is 29 with h_u . The existing solution is usually to install a single antenna on the train. As shown in Figure 3, the optimal number of antennas scheme provides a much higher capacity than the single antenna scheme.

In Figure 4, β indicates the attenuation of RF chain power. The mean value of cell capacity at different β is illustrated in the figure. 'X' marks the optimal operating point. For the DA system, the exhaustive search and Algorithm 1 are the sources of the optimal value of M . If the power attenuation in the RF chain is greater, both the most advantageous value M and the mean value cell capacity become smaller. When the most advantageous values of $M = 36$, $M = 30$, and $M = 25$ for co-located antenna and distributed antenna layouts, with $\beta = 0.4$ W, $\beta = 0.5$ W, and $\beta = 0.6$ W.

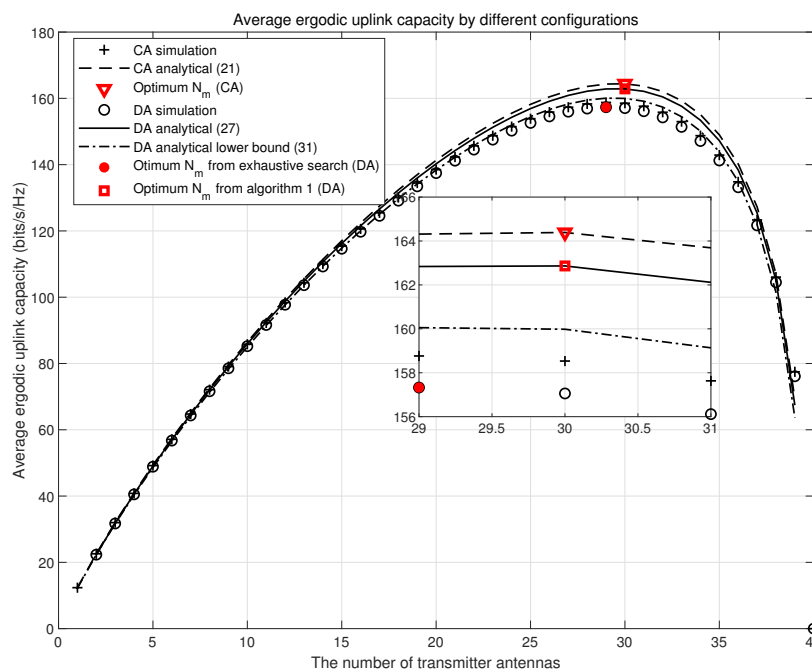


Figure 3. The mean value of capacity by different configuration.

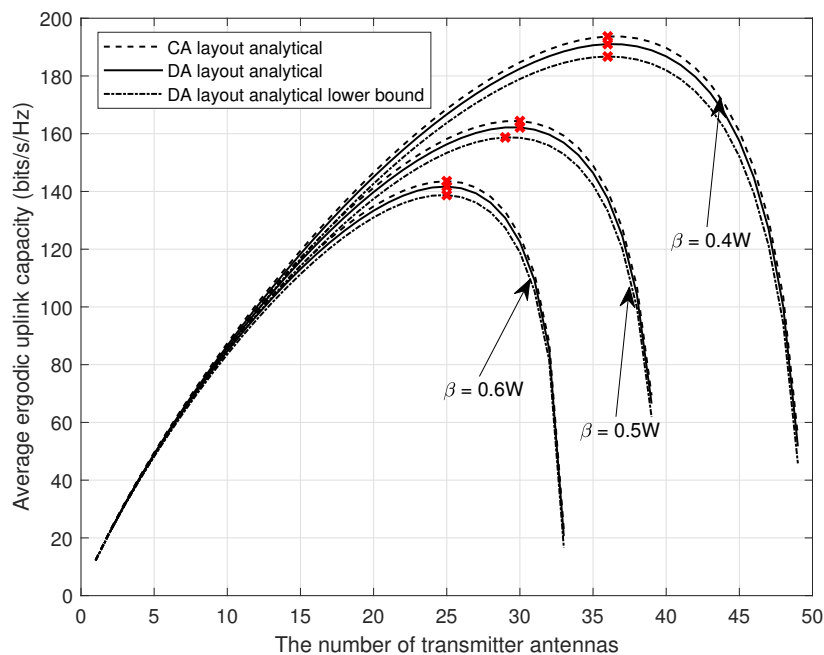


Figure 4. The mean value of up-link capacity by different RF power loss β .

In Figure 5, the ergodicity performance at a specific cellular location is depicted as a function of the train’s coordinate. We evaluated all system configurations using (16) to obtain the analysis results. CAs have different ergodic capacities in different environments. One is strong when in the center of the cell, and the other one is strong when it is far away from BS. The DA has a property that is important for providing stable quality of service throughout the cell. CA and DA layouts show smaller ergodic capacity fluctuations at unique cell locations. Increasing the length of a train reduces its top ergodic capacity but also produces less fluctuation in ergodic capacity.

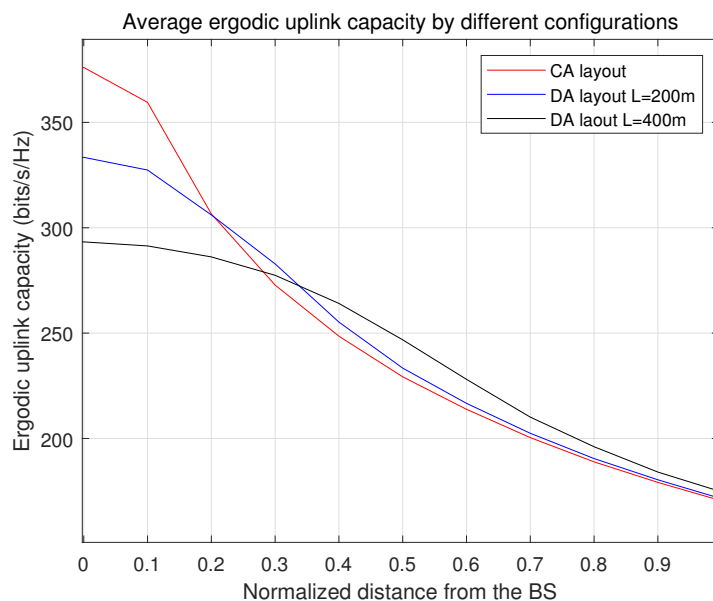


Figure 5. The capacity for different locations of train.

In Figure 6, the effect of the UAV altitude on the channel capacity is depicted for the same antenna layout and number of antennas. We have taken $h_u = 100, 200,$ and $300,$ respectively, at this point where $\beta = 0.5$ and $L = 200.$ As h_u becomes larger, the path loss decreases because the sum of the squares of distance d_x and height h_u becomes larger, resulting in both the direct and reflected paths becoming easier. As a result, the value of probability of LoS increases because direct paths are more likely to exist. As a result, the path loss dB decreases because more signals can reach the receiver directly. As a result, the cell radius increases because the signal strength can still exceed the signal threshold at greater distances. Additionally, it is easy to see that the average ergodic up-link capacity is smaller when h_u is larger.

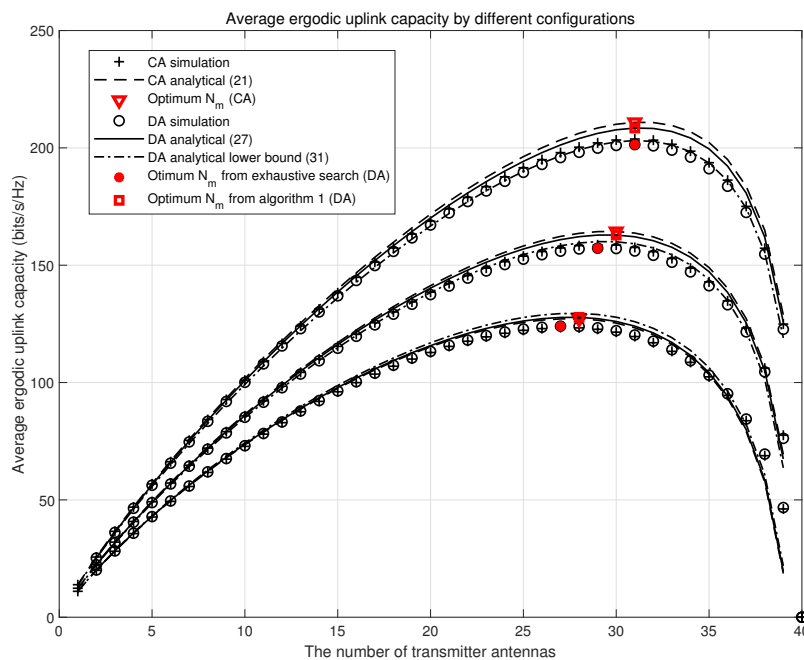


Figure 6. The mean value of capacity by different UAV heights $h_u.$

Table 3 shows the optimal antenna number comparison for CA and DA layouts for different K factors, with $\beta = 0.5$. Furthermore, it provides the benefits of the two layouts.

Table 3. Comparison of CA and DA layouts.

	CA Layout	DA Layout
Optimal Antenna for $K = 0$	31	31
Optimal Antenna for $K = 3$	28	29
Optimal Antenna for $K = 5$	27	28
Benefits	Higher average capacity	Higher capacity for cell edge

6. Conclusions

This system can be of great use in remote forests and in natural disaster environments. Combining smart reflectors with UAVs on a single platform can enhance spectrum and individual energy efficiency, expand network coverage, and provide flexible deployment options. The study investigated the design and performance of multiple-input-multiple-output systems using UAV-integrated reflective surfaces in high mobility scenarios for high-speed railway communication. In suburban environments, direct links between base stations and trains are often obstructed, particularly in mountainous areas. We conducted an experiment to address this issue. The evaluation and plan of massive MIMO for HSR communication is used in this work. The disadvantages of this system are: (1) The flight height and speed of the UAV are limited, which may affect the communication quality; (2) The flight time of the UAV is limited, and the battery needs to be replaced frequently; (3) The high cost of the UAV requires a large amount of investment. To calculate the mean value of the up-link cell capacity, we take into account not only the effects of large-scale fading and small-scale fading, but also the impact of RF power loss and the antennas' placement on top of the train. The optimal or sub-optimal approach was employed to optimize each cellular and distributed antenna system in order to determine the number of training antennas that maximize the mean value of the up-link cell capacity. Based on both numerical and simulation results, it can be concluded that the CA layout system has a better mean value for up-link cell capacity in comparison to the DA layout. In addition, when the distance from the BS is certain, the DA system exhibits a greater ergodic capacity. The DA layout has only a small variation in its ergodic ability at various locations within the cell. Furthermore, the lower number of transmitting antennas on the trains in the CA and DA arrangement is due to the higher UAV attitude. This is the expected result.

Author Contributions: Literature search, Study design and Manuscript writing, Z.L., J.C.; Graph production, Data analysis, Data processing, M.Y.; Supervision, Resources, review and editing, X.Z.; Translation, Literature search, Y.X.; All authors have read and agreed to the published version of the manuscript.

Funding: Sci. & Technol. Major Project of Tibetan Autonomous Region of China: XZ202201ZD0006G02; Fundamental Research Funds for the Central Universities: 2682023CX078; Natural Science Foundation of Sichuan Province under Grant 2023NSFSC1377.

Data Availability Statement: Not applicable.

Conflicts of Interest: The authors declare no conflict of interest.

References

1. Liu, X.; Qiao, D. Design and Coverage Analysis of Elliptical Cell Based Beamforming for HSR Communication Systems. In Proceedings of the ICC 2019—2019 IEEE International Conference on Communications (ICC), Shanghai, China, 20–24 May 2019; pp. 1–6. [\[CrossRef\]](#)
2. Xu, B.; Tong, Y.; Li, K.; Zhu, L.; Zheng, K.; Ma, S. Key Technology Research on Jointless Track Circuit in High-speed Railway. In Proceedings of the 2018 International Conference on Information Systems and Computer Aided Education (ICISCAE), Changchun, China, 6–8 July 2018; pp. 443–445. [\[CrossRef\]](#)

3. Hasegawa, F.; Taira, A.; Noh, G.; Hui, B.; Nishimoto, H.; Okazaki, A.; Okamura, A.; Lee, J.; Kim, I. High-Speed Train Communications Standardization in 3GPP 5G NR. *IEEE Commun. Stand. Mag.* **2018**, *2*, 44–52. [\[CrossRef\]](#)
4. Song, H.; Fang, X.; Fang, Y. Millimeter-Wave Network Architectures for Future High-Speed Railway Communications: Challenges and Solutions. *IEEE Wirel. Commun.* **2016**, *23*, 114–122. [\[CrossRef\]](#)
5. Han, S.; Chih-Lin, I.; Xie, T.; Wang, S.; Huang, Y.; Dai, L.; Sun, Q.; Cui, C. Achieving High Spectrum Efficiency on High Speed Train for 5G New Radio and Beyond. *IEEE Wirel. Commun.* **2019**, *26*, 62–69. [\[CrossRef\]](#)
6. Yang, J.; Ai, B.; Salous, S.; Guan, K.; He, D.; Shi, G.; Zhong, Z. An Efficient MIMO Channel Model for LTE-R Network in High-Speed Train Environment. *IEEE Trans. Veh. Technol.* **2019**, *68*, 3189–3200. [\[CrossRef\]](#)
7. Khallaf, H.S.; Uysal, M. UAV-Based FSO Communications for High Speed Train Backhauling. In Proceedings of the 2019 IEEE Wireless Communications and Networking Conference (WCNC), Marrakesh, Morocco, 15–18 April 2019; pp. 1–6. [\[CrossRef\]](#)
8. Li, T.; Tong, H.; Xu, Y.; Su, X.; Qiao, G. Double IRSs Aided Massive MIMO Channel Estimation and Spectrum Efficiency Maximization for High-Speed Railway Communications. *IEEE Trans. Veh. Technol.* **2022**, *71*, 8630–8645. [\[CrossRef\]](#)
9. Wu, Q.; Zhang, S.; Zheng, B.; You, C.; Zhang, R. Intelligent Reflecting Surface-Aided Wireless Communications: A Tutorial. *IEEE Trans. Commun.* **2021**, *69*, 3313–3351. [\[CrossRef\]](#)
10. Buzzi, S.; D’Andrea, C.; Zappone, A.; Fresia, M.; Zhang, Y.P.; Feng, S. RIS Configuration, Beamformer Design, and Power Control in Single-Cell and Multi-Cell Wireless Networks. *IEEE Trans. Cogn. Commun. Netw.* **2021**, *7*, 398–411. [\[CrossRef\]](#)
11. Zhang, J.; Du, H.; Zhang, P.; Cheng, J.; Yang, L. Performance Analysis of 5G Mobile Relay Systems for High-Speed Trains. *IEEE J. Sel. Areas Commun.* **2020**, *38*, 2760–2772. [\[CrossRef\]](#)
12. Ma, Y.; Niu, Y.; Han, Z.; Ai, B.; Li, K.; Zhong, Z.; Wang, N. Robust Transmission Scheduling for UAV-Assisted Millimeter-Wave Train-Ground Communication System. *IEEE Trans. Veh. Technol.* **2022**, *71*, 11741–11755. [\[CrossRef\]](#)
13. Wu, Q.; Sheng, J.; Wu, C.; Zhang, J.; Wang, Y. Research on UAV Networking Technology for High-speed Railway Emergency Communication. In Proceedings of the 2021 International Wireless Communications and Mobile Computing (IWCMC), Harbin, China, 28 June–2 July 2021; pp. 1557–1562. [\[CrossRef\]](#)
14. Chen, C.; Niu, Y.; Ai, B.; He, R.; Han, Z.; Zhong, Z.; Wang, N.; Su, X. Joint Design of Phase Shift and Transceiver Beamforming for Intelligent Reflecting Surface Assisted Millimeter-Wave High-Speed Railway Communications. *IEEE Trans. Veh. Technol.* **2022**, *72*, 6253–6267. [\[CrossRef\]](#)
15. Guo, Y.; Fang, F.; Cai, D.; Ding, Z. Energy-Efficient Design for a NOMA Assisted STAR-RIS Network With Deep Reinforcement Learning. *IEEE Trans. Veh. Technol.* **2022**, *72*, 5424–5428. [\[CrossRef\]](#)
16. Zhang, J.; Liu, H.; Wu, Q.; Jin, Y.; Chen, Y.; Ai, B.; Jin, S.; Cui, T.J. RIS-Aided Next-Generation High-Speed Train Communications: Challenges, Solutions, and Future Directions. *IEEE Wirel. Commun.* **2021**, *28*, 145–151. [\[CrossRef\]](#)
17. Zhang, Q.; Saad, W.; Bennis, M. Reflections in the Sky: Millimeter Wave Communication with UAV-Carried Intelligent Reflectors. In Proceedings of the 2019 IEEE Global Communications Conference (GLOBECOM), Big Island, HI, USA, 9–13 December 2019; pp. 1–6. [\[CrossRef\]](#)
18. Mohamed, Z.; Aïssa, S. Leveraging UAVs with Intelligent Reflecting Surfaces for Energy-Efficient Communications with Cell-Edge Users. In Proceedings of the 2020 IEEE International Conference on Communications Workshops (ICC Workshops), Virtual, 7–11 June 2020; pp. 1–6. [\[CrossRef\]](#)
19. Pang, X.; Sheng, M.; Zhao, N.; Tang, J.; Niyato, D.; Wong, K.K. When UAV Meets IRS: Expanding Air-Ground Networks via Passive Reflection. *IEEE Wirel. Commun.* **2021**, *28*, 164–170. [\[CrossRef\]](#)
20. Li, Y.; Zhang, H.; Long, K.; Nallanathan, A. Exploring Sum Rate Maximization in UAV-Based Multi-IRS Networks: IRS Association, UAV Altitude, and Phase Shift Design. *IEEE Trans. Commun.* **2022**, *70*, 7764–7774. [\[CrossRef\]](#)
21. Li, K.; Zhao, K.; Khan, M.F.; Ho, P.H.; Peng, L. UAV-mounted Intelligent Reflecting Surface (IRS) MISO Communications. In Proceedings of the 2022 International Conference on Networking and Network Applications (NaNA), Qingdao, China, 3–5 December 2022; pp. 62–66. [\[CrossRef\]](#)
22. Shafique, T.; Tabassum, H.; Hossain, E. Optimization of Wireless Relaying With Flexible UAV-Borne Reflecting Surfaces. *IEEE Trans. Commun.* **2021**, *69*, 309–325. [\[CrossRef\]](#)
23. Liu, Z.; Wu, J.; Fan, P. On the Uplink Capacity of High Speed Railway Communications with Massive MIMO Systems. In Proceedings of the 2014 IEEE 79th Vehicular Technology Conference (VTC Spring), Seoul, Republic of Korea, 18–21 May 2014; pp. 1–5. [\[CrossRef\]](#)
24. Zhang, J.; Dai, L.; He, Z.; Jin, S.; Li, X. Performance Analysis of Mixed-ADC Massive MIMO Systems Over Rician Fading Channels. *IEEE J. Sel. Areas Commun.* **2017**, *35*, 1327–1338. [\[CrossRef\]](#)
25. Wang, Y.; Niu, Y.; Wu, H.; Mao, S.; Ai, B.; Zhong, Z.; Wang, N. Scheduling of UAV-Assisted Millimeter Wave Communications for High-Speed Railway. *IEEE Trans. Veh. Technol.* **2022**, *71*, 8756–8767. [\[CrossRef\]](#)
26. Huang, Q.; Hu, A. Channel estimation via GAMP for millimeter wave hybrid massive MIMO systems. *Frequenz* **2022**, *76*, 351–360. [\[CrossRef\]](#)
27. Alzenad, M.; El-Keyi, A.; Lagum, F.; Yanikomeroglu, H. 3-D placement of an unmanned aerial vehicle base station (UAV-BS) for energy-efficient maximal coverage. *IEEE Wirel. Commun. Lett.* **2017**, *6*, 434–437. [\[CrossRef\]](#)
28. Al-Hourani, A.; Kandeepan, S.; Lardner, S. Optimal LAP altitude for maximum coverage. *IEEE Wirel. Commun. Lett.* **2014**, *3*, 569–572. [\[CrossRef\]](#)

29. Soret, B.; Aguayo-torres, M.C.; Entrambasaguas, J.T. Capacity with Explicit Delay Guarantees for Generic Sources over Correlated Rayleigh Channel. *IEEE Trans. Wirel. Commun.* **2010**, *9*, 1901–1911. [[CrossRef](#)]
30. Telatar, E. Capacity of Multi-antenna Gaussian Channels. *Eur. Trans. Telecomm.* **1999**, *10*, 585–595. [[CrossRef](#)]
31. Liu, Z.; Wu, J.; Fan, P. Performance analysis and antenna selection of high speed railway communications systems with distributed antennas. In Proceedings of the 2014 International Workshop on High Mobility Wireless Communications, Beijing, China, 1–3 November 2014; pp. 7–11. [[CrossRef](#)]

Disclaimer/Publisher’s Note: The statements, opinions and data contained in all publications are solely those of the individual author(s) and contributor(s) and not of MDPI and/or the editor(s). MDPI and/or the editor(s) disclaim responsibility for any injury to people or property resulting from any ideas, methods, instructions or products referred to in the content.